Soft Matter

RSC Publishing

COMMUNICATION

View Article Online
View Journal | View Issue

Cite this: *Soft Matter*, 2013, **9**, 6033

The effect of pH on the self-assembly of a collagen derived peptide amphiphile†

Ashkan Dehsorkhi,[a] Valeria Castelletto,[a] Ian W. Hamley,*[a] Jozef Adamcik[b] and Raffaele Mezzenga*[b]

Received 15th April 2013
Accepted 22nd May 2013

DOI: 10.1039/c3sm51029h

www.rsc.org/softmatter

Transitions in nanostructure driven by pH are observed for a self-assembling peptide amphiphile (PA) with a cationic pentapeptide headgroup. At pH 3, the PA forms flat tape-like structures, while at pH 4 the PA assembles into twisted right handed structures. These twisted structures transform again to flat tape-like structures at pH 7. In complete contrast, spherical micelles are observed at pH 2. These changes in response to pH may be relevant to biological and pharmaceutical applications of this PA in skincare.

Peptide amphiphiles (PAs) are remarkable molecules in which the biofunctionality of peptides is controlled by the amphiphilicity imparted by attachment of lipid chains. This leads to novel nanostructures with the possibility to fine tune the balance of hydrogen bonding with hydrophobic and electrostatic interactions, which together govern the peptide self-assembly. There is unprecedented scope to further utilize this to generate self-assembled structures with hierarchical ordering due to interactions with other functional molecules.

Here, we investigate the influence of pH on the self-assembly of the PA C_{16}-KTTKS which has a pentapeptide headgroup based on a sequence from pro-collagen I. C_{16}-KTTKS is used commercially (under the trade name Matrixyl) in anti-wrinkle creams. The pH of skin is slightly acidic (values in the range pH 4–6 have been reported)[1–3] and therefore the effect of pH on the self-assembly and activity of PA may be relevant to its application, to date in cosmetics but potentially also in wound healing. Indeed, conditions such as acne and eczema can influence the pH of the skin, and can damage it, as can the aging process. Melanoma (skin cancer) is an even more severe disease and it is typically associated with reduced skin pH.[4] It is therefore of practical as well as fundamental interest to examine the pH dependence of the self-assembly of a PA used in skincare applications. The formation of giant extended nanotapes by PAs has been observed using several microscopic methods.[5,6] Small-angle X-ray scattering (SAXS) indicates that the tapes comprise bilayers of the peptide amphiphile molecules. The polar head of C_{16}-KTTKS, has a net charge of +2 at low pH and +1 at pH 7, due to the presence of the two lysine residues and the carboxy terminus. We have also previously investigated electrostatic effects on the interaction of this PA with the anionic surfactant sodium dodecyl sulphate (SDS) and observed that in the presence of the surfactant, tapes are disrupted and fine twisted fibrils can be produced.[7]

The structures formed after the self-assembly of C_{16}-KTTKS at the different pH investigated in this study were evaluated by atomic force microscopy (AFM). Fig. 1 shows the AFM images for 1 wt% solutions of C_{16}-KTTKS at pH 2 (Fig. 1a), at native pH 3 (Fig. 1c), at pH 4 (Fig. 1d) and at pH 7 (Fig. 1e). 3D AFM images of those images are shown in ESI Fig. 1.† From the AFM images it is clear that different morphological structures of C_{16}-KTTKS are formed at different pHs. Additional AFM images for 1 wt% solutions of C_{16}-KTTKS at pH 3, 4 and 7 are shown in ESI Fig. 2.† At native pH 3 multilayered flat-tape structures are observed (Fig. 1c) as previously reported.[7] The longitudinal height profile of the tapes confirms a flat surface of these structures (Fig. 1f, blue curve). However, at just slightly higher pH, *i.e.* pH 4, the presence of twisted fibrillar structures is detected (Fig. 1d). All the twisted fibrillar structures are right handed with the longitudinal height profile (Fig. 1f, black curve) typical for twisted structures such as amyloid fibrils.[8] Upon an increase in pH from pH 4 to pH 7, obtained by adding NaOH, a change in morphology again occurs, with flat tape structures appearing (Fig. 1e) similar to the structures assembled at native pH 3. Completely different structures were detected in the case of 1 wt% C_{16}-KTTKS at pH 2 (by adding HCl to a pH 4 solution) as compared to pH 3, 4 and 7, since spherical micellar structures could be observed (Fig. 1a). The statistical analysis of the height of the micelles is presented in Fig. 1b and the height of the

[a]*Dept of Chemistry, University of Reading, Whiteknights Reading RG6 6AD, UK. E-mail: I.W.Hamley@reading.ac.uk*

[b]*Food & Soft Materials Science, ETH Zürich, Schmelzbergstrasse 9, 8092 Zürich, Switzerland. E-mail: raffaele.mezzenga@hest.ethz.ch*

† Electronic supplementary information (ESI) available: Experimental methods and characterization data. Additional experimental data. See DOI: 10.1039/c3sm51029h

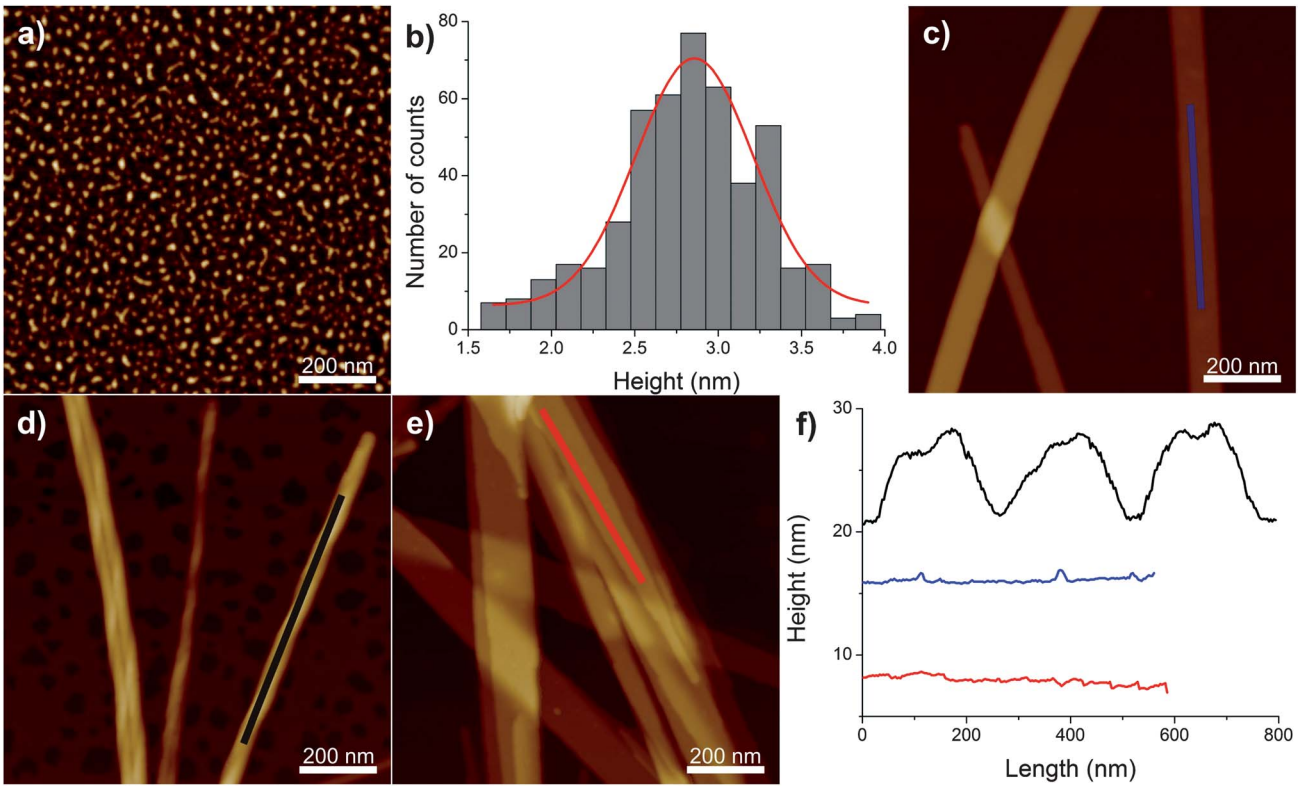

Fig. 1 (a) AFM image of 1 wt% C_{16}-KTTKS at pH 2. (b) The height distribution for spherical micelles extracted from the AFM images of 1 wt% C_{16}-KTTKS at pH 2. AFM images of 1 wt% C_{16}-KTTKS at: (c) native pH 3, (d) pH 4 and (e) pH 7. (f) The longitudinal height profiles of the structures observed for 1 wt% C_{16}-KTTKS at native pH 3 (blue curve), at pH 4 (black curve) and at pH 7 (red curve). *Z* scale for the AFM images is 6 nm for (a) and 60 nm for (c–e).

micelles was determined to be 2.7–2.8 nm. Thus, AFM reveals a transition in morphology upon increase in pH from spherical micelles (pH 2) to flat tapes (pH 3) to twisted fibrous tapes (pH 4) to flat broad tapes (pH 7).

SAXS was employed to further elucidate the self-assembled nanostructures in aqueous solution, and the main results are summarized in Fig. 2.

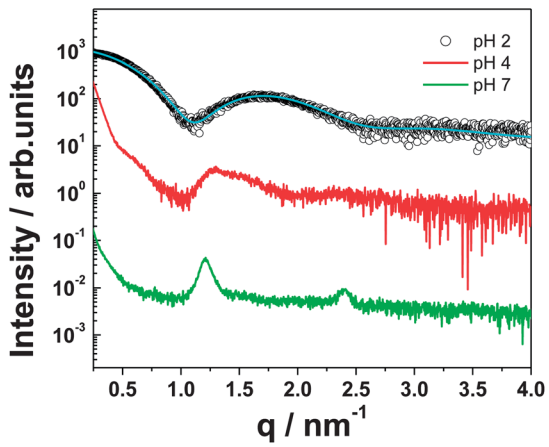

Fig. 2 SAXS profiles for 1 wt% C_{16}-KTTKS at pH 2, pH 4 and pH 7. The solid line through the data for the pH 2 sample is a fit to a form factor for spherical micelles, as described in the text and in the ESI.†

Peaks for the pH 7 sample were observed at 1.2 nm^{-1} and 2.4 nm^{-1}. This is indicative of a bilayer structure of the nanotapes of C_{16}-KTTKS (d = 5.24 nm) as previously reported.[5,9] In direct support of the SAXS results, a value of 5.3 nm for the height of thinnest nanotapes was also obtained by AFM at pH 7, confirming the bilayer spacing measured by scattering and in perfect agreement with the results reported in our previous work.[7] A similar SAXS profile is obtained for C_{16}-KTTKS at pH 4, which lacks a second order lamellar reflection, but nonetheless still exhibits the main bilayer spacing as for pH 7. At pH 2, neglecting the influence of structure factor in the scattering profile in this q-range, the form factor was fitted to a spherical micelle model as shown in Fig. 2 (see ESI for details†), which supports the findings from the AFM measurements shown in Fig. 1a. Recently we reported for C_{16}-KTTKS the transition from nanotape fibrils to spherical micelles with an increase in temperature to 55 °C.[9] Similarly, we observe here a similar transition but this time with a decrease in pH. The pH of C_{16}-KTTKS was measured at room temperature and was found to be pH 3. Interestingly, increasing the temperature to 55 °C caused a reduction in pH to pH 2.38. The fitting parameters for the pH 2 curve (provided in the ESI†) are strikingly similar to the data for the native pH sample at 55 °C, which is, again, consistent with the formation of spherical micelles.[9] The charge of the PA was calculated using the software HySS. This revealed an increase in charge as pH decreases. At pH 7, the charge was calculated to be +1.00e increasing to a charge of +1.51e at pH 3

and +1.91e at pH 2, *i.e.* with a larger relative change in charge between pH 3 and pH 2 corresponding to the micelle–tapes transition.

The breakdown of tape-like elongated aggregates into small micelles can be understood by drawing a direct analogy with the behaviour of hydrophobic polyelectrolytes (*i.e.* polyelectrolytes in a poor solvent). In hydrophobic polyelectrolytes, a transition from a globular structure to a necklace configuration formed by strings-and-beads is observed when the linear charge density exceeds a well-defined critical value. In the present case, a breakdown of an elongated fibrillar/tape-like object into smaller micelles can be expected when the electrostatic energy per unit length (promoting dissociation) exceeds the cohesive energy per unit length, the latter comprising the surface tension and β-sheet hydrogen bonds (holding together the fibril):

$$k_B T l_B (N_{charges})^2/L > \sigma\pi D_{equivalent} L + \Delta F_{\beta\text{-sheets}} L \quad (1)$$

where k_B is the Boltzmann constant, T is the temperature, l_B is the Bjerrum length, $N_{charges}$ is the total number of charges per length L, σ is the fibril–water interfacial tension, $\pi D_{equivalent}$ is the cross-sectional perimeter of the fibril ($D_{equivalent}$ being the diameter of the cylindrical fibril with an equivalent cross-sectional perimeter) and $\Delta F_{\beta\text{-sheets}}$ is the total energy per length L due to β-sheet H-bonds. Eqn (1) can be reworked into:

$$\lambda_{critic}{}^2 > (\sigma\pi D_{equivalent} + \Delta F_{\beta\text{-sheets}})/k_B T l_B \quad (2)$$

where $\lambda_{critic} = N_{charges}/L$ is the critical linear charge density at which the electrostatic breakdown is expected. The right term in eqn (2) is dependent on the temperature, shape, topology and composition of the fibril. Thus, for a given fibril shape, eqn (2) predicts an electrostatic breakdown of the fibril at a given λ_{critic}, *i.e.* at a given pH, in agreement with AFM observation, which show a breakdown at pH between 3 and 2.

The transitions in nanostructures observed by AFM upon variation of pH for C_{16}-KTTKS solutions are supported by observations from circular dichroism (CD) spectroscopy. Fig. 3 shows CD spectra, which reveal the presence of β-sheet structures for 1 wt% C_{16}-KTTKS at native pH 3, as noted by us previously.[5]

CD spectra for both pH 4 and 7 also exhibit β-sheet features, which arise from the intermolecular hydrogen bonding between the pentapeptide headgroup, as highlighted by the minimum at 220 nm and a maximum at 195 nm.[10] In order to form high aspect ratio structures such as nanotapes and twisted fibres as shown by AFM, β-sheet ordering is required to stabilise the structure, as indicated by CD.[11] In contrast, the CD spectrum for 1 wt% C_{16}-KTTKS at pH 2 lacks β-sheet features and instead reveals a random coil spectrum with a minimum at 195 nm.[10] This is consistent with both the AFM images and SAXS analysis, again supporting the spherical micelle structures.

Fibre X-ray diffraction (XRD) was performed on dried stalks to complement *in situ* SAXS. XRD 2D images for 1 wt% C_{16}-KTTKS at pH 2, 4 and 7 are shown in ESI Fig. 3.† One-dimensional radial intensity profiles were obtained for all three pH values and shown in Fig. 4 in order to determine the *d*-spacing.

The 2D patterns for 1 wt% C_{16}-KTTKS at pH 3–7 indicate features of a cross-β sheet structure. A meridional reflection is present with $d = 4.69$ Å for pH 3–4, which corresponds to the spacings of the β-strands of the peptide headgroups.[12] A similar intensity profile for pH 7 is observed with a meridional reflection at $d = 4.76$ Å. The one-dimensional intensity profile for pH 2 lacks peaks corresponding to a cross-β sheet arrangement due to spherical micelle formation, consistent with AFM images and SAXS. Instead a sharp peak with $d = 2.83$ Å is observed. This is also observed for pH 3, 4 and 7, and relates to the local ordering of the PA assemblies. A peak at 3.16–3.27 Å is observed for the tape/fibril samples and is associated with lipid chain order.

Other authors have reported pH effects on PA self-assembly.[13–18] A few examples include the finding that the PA C_{12}-Aβ(11–17) self-assembles into fibrils at pH 3 and nanoribbons at pH 10.[14,15] The Stupp group has investigated the self-assembly of C_{16}-RGD, which formed long fibres at pH 4 and disassembled with an increase in pH.[16] Lin *et al.* have studied hydrogel formation of a self-assembled PA, C_{16}-GSH.[17] At pH 4 a network of entangled fibres are observed. As the pH increases a transition occurs to rods and ribbons. Ghosh *et al.* have reported a transition from fibrils to spherical micelles for the PA palmitoyl–IAAAEEEEK(DO3A:Gd)–NH_2, which occurs around

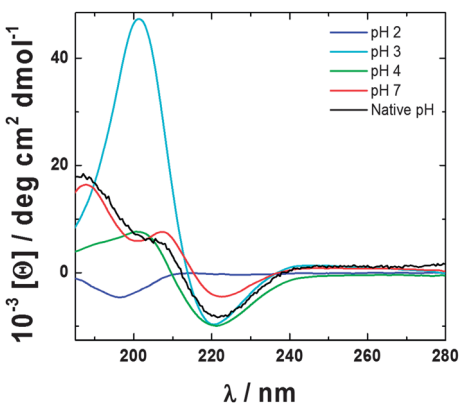

Fig. 3 CD spectra for 1 wt% C_{16}-KTTKS at varying pH as indicated.

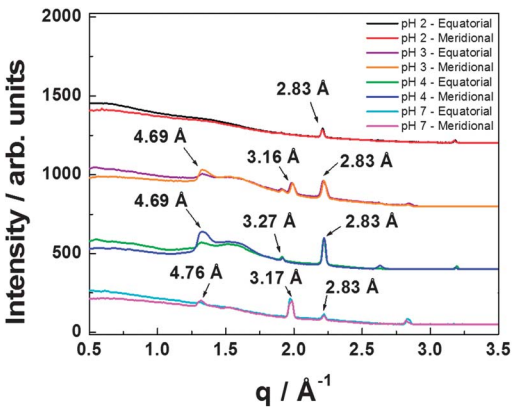

Fig. 4 XRD one-dimensional radial averages with indicated *d*-spacings for 1 wt% C_{16}-KTTKS at different pH values.

pH 6; in that case a DO3A group was incorporated into the PA molecule to influence self-assembly.[18] To our knowledge, this is the first report in which pH changes allow, within the same PA system, such a vast polymorphic control of the self-assembled structures, with morphology variations following the sequence upon pH increase: spherical micelles → flat tapes → twisted right handed fibrils → flat tapes.

In summary, we have shown that the self-assembly of C_{16}-KTTKS can be fine tuned by adjusting the pH of the solution. We observe that as the pH decreases a transition in morphology occurs from tapes, to twisted fibrils, to tapes, to micelles. While the break-down of tapes into spherical micelles at very low pH is understood based on electrostatic considerations, the fibril–tape transition sequence still needs to be fully elucidated and will be the topic of future studies. The solutions studied at pH 4 and 7 correspond to the range of pH values for skin, and under these conditions tapes and fibrils are expected to occur. Very low pH (pH 2) is not expected for skin and therefore micelles should not be observed in standard formulations. Studying the effects of pH on the self-assembly of a collagen stimulating PA is important as this molecule can play an important role in wound healing and regenerative medicine. We aim to shed light on this effect in order to improve skincare products for the future.

Notes and references

1 H. C. Korting and O. Braun-Falco, *Clin. Dermatol.*, 1996, **14**, 23.
2 G. Yosipovitch, E. Tur, O. Cohen and Y. Rusecki, *Diabetes Care*, 1993, **16**, 560.
3 H. Lambers, S. Piessens, A. Bloem, H. Pronk and P. Finkel, *Int. J. Cosmet. Sci.*, 2006, **28**, 359.
4 I. Parolini, C. Federici, C. Raggi, L. Lugini, S. Palleschi, A. De Milito, C. Coscia, E. Iessi, M. Logozzi, A. Molinari, M. Colone, M. Tatti, M. Sargiacomo and S. Fais, *J. Biol. Chem.*, 2009, **284**, 34211.
5 V. Castelletto, I. W. Hamley, J. Perez, L. Abezgauz and D. Danino, *Chem. Commun.*, 2010, **46**, 9185.
6 H. Cui, T. Muraoka, A. G. Cheetham and S. I. Stupp, *Nano Lett.*, 2009, **9**, 945.
7 V. Castelletto, I. W. Hamley, J. Adamcik, R. Mezzenga and J. Gummel, *Soft Matter*, 2012, **8**, 217.
8 J. Adamcik and R. Mezzenga, *Curr. Opin. Colloid Interface Sci.*, 2012, **17**, 369.
9 J. F. Miravet, B. Escuder, M. D. Segarra-Maset, M. Tena-Solsona, I. W. Hamley, A. Dehsorkhi and V. Castelletto, *Soft Matter*, 2013, **9**, 3558.
10 R. W. Woody, *Circular dichroism of peptides and proteins*, New York, 1994.
11 S. E. Paramonov, J. Ho-Wook and J. D. Hartgerink, *J. Am. Chem. Soc.*, 2006, **128**, 7291.
12 K. E. Marshall and L. C. Serpell, *Open Biol. J.*, 2009, **2**, 185.
13 J. Zhang, R. Hao, L. Huang, J. Yao, X. Chen and Z. Shao, *Chem. Commun.*, 2011, **47**, 10296.
14 M. Deng, D. Yu, Y. Hou and Y. Wang, *J. Phys. Chem. B*, 2009, **113**, 8539.
15 Y. Yan, Y. Lin, Y. Qiao and J. Huang, *Soft Matter*, 2011, **7**, 6385.
16 J. D. Hartgerink, E. Beniash and S. I. Stupp, *Science*, 2001, **294**, 1684.
17 B. F. Lin, K. A. Megley, N. Viswanathan, D. V. Krogstad, L. B. Drews, M. J. Kade, Y. Qian and M. V. Tirrell, *J. Mater. Chem.*, 2012, **22**, 19447.
18 A. Ghosh, M. Haverick, K. Stump, X. Yang, M. F. Tweedle and J. E. Goldberger, *J. Am. Chem. Soc.*, 2012, **134**, 3647.